separated in detail, and it was found that the relaxation of those voltage losses appeared at different time regions. It was demonstrated that each voltage loss is easily determined at once with one-shot experiments of the current interruption.

The analysis of η_{Re} indicates that the oxygen reduction process in a 100 cm^2 class MCFC is under mixed diffusion of superoxide ion (O_2^-) and CO_2.

Acknowledgment

This work is partly supported by International Joint Research Grant (Advance MCFC) of New Energy and Industrial Technology Development Organization (NEDO).

Manuscript submitted August 25, 1997; revised manuscript received April 28, 1998.

Tohoku University, assisted in meeting the publication costs of this article.

REFERENCES

1. K. Ota, Y. Takeishi, S. Shibata, H. Yoshitake, and N. Kamiya, *J. Electrochem. Soc.*, **142**, 3322 (1995).
2. J. R. Selman and H. C. Maru, in *Advances in Molten Salt Chemistry*, Vol. 4, G. Mamantov and J. Braunstein, Editors, Plenum Press, New York (1983).
3. T. Nishina, Y. Masuda, and I. Uchida, in *Molten Salt Chemsitry and Technology*, M.-L. Saboungi and H. Kojima, Editors, PV 93-9, p. 424, The Electrochemical Society Proceedings Series, Pennington, NJ (1993).
4. A. J. Appleby and S. B. Nicholson, *J. Electroanal. Chem.*, **53**, 105 (1974).
5. A. J. Appleby and S. B. Nicholson, *J. Electroanal. Chem.*, **83**, 309 (1977).
6. A. J. Appleby and S. B. Nicholson, *J. Electroanal. Chem.*, **112**, 71 (1980).
7. T. Nishina, I. Uchida, and J. R. Selman, *J. Electrochem. Soc.*, **141**, 1191 (1994).
8. J. H. Hirschenhofer, D. B. Stauffer, and R. R. Engleman, *Fuel Cells A Handbook*, U.S. Department of Energy, DOE/METEC-94/1006, Washington, DC (1994).
9. T. G. Benjamin, E. H. Camara, and L. G. Marianowski, *Handbook of Fuel Cell Performance*, p. 37, U.S. Department of Energy, C00-1545-T1, Washington, DC (1980).
10. V. Sampath, A. F. Sammells, and J. R. Selman, *J. Electrochem. Soc.*, **127**, 79 (1980).
11. Y. Mugikura, T. Abe, T. Watanabe, and Y. Izaki, *Denki Kagaku oyobi Kogyo Butsuri Kagaku*, **60**, 124 (1992).
12. Y. Miyazaki, M. Yanagida, S. Tanase, K. Tanimoto, T. Kojima, N. Ohtori, H. Okuyama, and T. Kodama, *Denki Kagaku oyobi Kogyo Butsuri Kagaku*, **60**, 816 (1992).
13. C. Y. Yuh and J. R. Selman, *J. Electrochem. Soc.*, **138**, 3642 (1991).
14. C. Lagergren, G. Lindbergh, and D. Simonsson, *J. Electrochem. Soc.*, **142**, 787 (1995).
15. E. Yeager and J. Kuta, in *Physical Chemistry: An Advanced Treatise*, Vol. IX A, H. Eyring, D. Henderson, and W. Jost, Editors, p. 369, Academic Press, New York (1970).
16. P. G. P. Ang and A. F. Sammells, *J. Electrochem. Soc.*, **127**, 1287 (1980).
17. T. Nishina, M. Takahashi, and I. Uchida, *J. Electrochem. Soc.*, **137**, 1112 (1990).
18. A. J. Bard and L. R. Faulkner, *Electrochemical Methods: Fundamentals and Applications*, John Wiley & Sons, Inc., New York (1980).
19. H. Morita, Y. Mugikura, Y. Izaki, T. Watanabe, and T. Abe, in *Carbonate Fuel Cell Technology*, J. R. Selman, I. Uchida, H. Wendt, D. A. Shores, and T. F. Fuller, Editors, PV 97-4, p. 151, The Electrochemical Society Proceedings Series, Pennington, NJ (1997).
20. C. G. Lee, H. Nakano, T. Nishina, I. Uchida, Y. Izaki, and S. Kuroe, *Denki Kagaku oyobi Kogyo Butsuri Kagaku*, **64**, 486 (1996).

Lithium Insertion in Carbon–Silicon Composite Materials Produced by Mechanical Milling

C. S. Wang,*[a] G. T. Wu,[b] X. B. Zhang,[a] Z. F. Qi,[b] and W. Z. Li[b]

[a]*Department of Materials Science and Engineering, and* [b]*Department of Physics, Zhejiang University, Hangzhou 310027, China*

ABSTRACT

Carbons containing nanosize silicon particles were prepared by mechanical milling of graphite and silicon mixtures with different atomic ratios. The microstructure, morphology, and electrochemical performance of ballmilled $C_{1-x}Si_x$ (x = 0, 0.1, 0.2, 0.25) were analyzed by X-ray diffraction, Raman, high-resolution and transmission electron microscopy, and electrochemical methods. After ballmilling, the crystal size of graphite increased but the size of silicon decreased with increasing content of silicon. Ballmilled $C_{1-x}Si_x$ materials reacted reversibly with lithium, and the reversible specific capacity increased from 437 mAh/g in the ballmilled pure graphite to 1039 mAh/g in ballmilled $C_{0.8}Si_{0.2}$ materials. The excess capacity due to the Li extraction from silicon appeared at a potential about 0.4 V vs. Li metal. After 20 charge/discharge cycles the reversible capacity of $C_{0.8}Si_{0.2}$ was 794 mAh/g. This behavior is a result of nanosize silicon particles decreasing the crumbling rate during Li insertion and extraction. These materials appear to be promising candidates for negative electrodes in lithium-ion rechargeable batteries.

Introduction

The search for the best carbon negative-electrode (anode) materials for lithium-ion batteries is a worldwide effort which will ultimately affect the energy density and performance of lithium-ion batteries. Graphite is the most studied host. It can be intercalated to a maximum of one lithium per six carbons under ambient-temperature conditions.

One method to improve the capacity of graphite is mixing alloying elements with graphite, either substitutionally or additionally. Silicon, lead, and tin each form alloys with lithium to a limit of at least three lithium atoms per heavy atom.[1,2] However, the alloying process does not appear to be sufficiently reversible for direct replacement of graphite electrode materials in spite of the greater capacity of the alloys for lithium.[2] The limited cycling capacity is related to the crumbling of alloy materials due to large volume expansion during lithium insertion and brittleness of the intermetallic lithium phase (Zintl phase).[3] Because silicon crystals can be intercalated to a maximum of 4.4 lithium atoms per silicon atom[2] and the crumbling rate may be slower if the silicon host particles are nanosized,[3] it is our idea that the benefits of carbon–silicon composite materials, i.e., the high volumetric energy density of silicon and

* Electrochemical Society Active Member.

the reversibility of the graphite could be realized if nanosized silicon crystals were dispersed throughout a graphite host. The carbon and silicon may have a different tendency to accommodate lithium. When Li is inserted in C/Si composite hosts, the expansion of the Si–Li alloy can be accommodated by relatively soft and ductile graphite (or graphite intercalation compound). Carbons containing nanodispersed silicon atoms produced by the chemical vapor deposition (CVD) method have been reported by Wilson et al.[4] The results show that the capacity is near 500 mAh/g, which is 1.5 times the capacity of graphite. The shortcoming of the CVD method is the difficulty in controlling composition and obtaining homogeneous materials.[4] Also, if the content of silicon exceeds 11 atom %, SiC is formed.[4]

Mechanical milling/alloying has been shown to be a powerful technique to produce controlled composition and sized powders with a homogeneous structure in different alloy systems, which is difficult to obtain with the CVD method. The starting materials employed for the mechanical milling process are single phase, whereas those for mechanical alloying are typically two or more phases. It has been discovered that mechanical ballmilling can be used to obtain crystal-to-amorphous and/or crystal-to-nanocrystallite transitions for semiconductor elements, e.g., C[5,6] and Si.[7,8] Recently, Yang and Shaw[9] have investigated the alloying process through high-energy mechanical milling of elemental silicon and carbon mixtures with an atomic ratio of 1:1.

The electrochemical performance of graphite and soft carbon produced by mechanical milling was studied by Disma et al.,[10] who found that the milled graphite and soft carbon can intercalate reversibly up to two lithiums per six carbons (e.g., Li_2C_6) while having irreversible capacities of 328 mAh/g. Here we synthesized carbons containing nanosize silicon particles by a mechanical alloying method and studied their crystallite size, morphology, and electrochemical performance when they were used as electrodes in Li/C cells.

Experimental

Preparation of ballmilled $C_{1-x}Si_x$ (x = 0, 0.1, 0.2, 0.25) powder.—The ballmilling was carried out in a conventional planetary ball mill. Powder mixtures of pure graphite (99.9%, −325 mesh) and crystalline silicon (99.5%, −325 mesh) with different atomic ratios ($C_{1-x}Si_x$, x = 0–0.25) were placed in a hard bearing steel vial under a dry pure argon atmosphere. The steel vial was sealed with an elastic O-ring seal, and the ballmilling was performed for 150 h without interruption. The weight ratio of the steel ball to powder mixture was 12:1, and the rotation rate of the vial was 270 rpm.

X-ray diffraction and Raman spectra measurements.—The structures of ballmilled $C_{1-x}Si_x$ (x = 0, 0.1, 0.2, 0.25) and unmilled $C_{0.6}Si_{0.4}$ powder were analyzed by X-ray diffraction (XRD) measurements using a Philips diffractometer PW 1710 with Cu Kα radiation (1.5418 Å). The crystallite size *Lc*, of carbon was determined from the [002] Bragg peak using the Scherrer equation[11]

$$L_{hkl} = 0.9\lambda/(\beta \cos\theta)$$

where λ is the X-ray wavelength, θ is the Bragg angle, and β is the real half-peak width in radians after corrections for instrument broadening. The full width at half intensity, β_{exp}, was first measured, and then the instrumental broadening, β_{inst}, was subtracted ($\beta = \sqrt{\beta^2_{exp} - \beta^2_{inst}}$) to obtain β. The Raman spectra (RS) were excited with 150 mW of 514.5 nm radiation from an Ar-ion laser, and the scattered light was dispersed with a V1000 ISA double spectrometer. The sample geometry for the RS measurements was a disk with a diameter of 3 mm and a thickness of 0.5 nm prepared by pressing the powder under a nominal pressure of 3.1 Gpa.

High-resolution and transmission electron microscopy observations.—The microstructure and morphology observations were performed in a side-entry JEOL2010 high-resolution electron microscope with a point-to-point resolution of 0.19 nm and a JEOL200CX transmission electron microscope. The ballmilled powders prepared for high-resolution electron microscopy (HREM) and transmission electron microscopy (TEM) observation were first dispersed in alcohol and then dropped onto carbon-coated copper grids.

Electrochemical testing.—All electrochemical measurements were carried out using coin-type test cells. The working electrodes were made from unmilled graphite and ballmilled $C_{1-x}Si_x$ (x = 0, 0.1, 0.2, 0.25) powder. Polytetrafluoroethylene (PTFE) diluted in anhydrous alcohol was added into the mixed powders such that approximately 8% of the final electrode mass was PTFE. Excess anhydrous alcohol was added until the slurry reached a smooth, syrupy viscosity. The slurry was then spread uniformly onto preweighed foam nickel. Once the electrode was dried, it was compressed between flat plates to ~30 bar pressure, dried at 150°C under vacuum overnight, and then weighed to determine the active mass of carbon. The electrodes usually had an active mass of 16 mg. A microporous separator film which had been wetted with 1 M $LiClO_4$ dissolved in a 50/50 (v/o) mixture of ethylene carbonate (EC) and diethyl carbonate (DEC) was sandwiched between the working electrode and a Li metal foil anode. The electrode was then wet with the same electrolyte as the separator. Half-cells were assembled in an argon-filled glove box.

Additionally, electrodes of 60 atom % graphite (unmilled) and 40 atom % silicon (unmilled) powder were made by the method outlined for comparison with the ballmilled $C_{1-x}Si_x$ electrodes. The electrode was charged/discharged using constant current between 0.005 and 1.5 V at room temperature. For the first charge/discharge and second charge the electrode was cycled using a constant current of 15 mA/g. A lower cycling current of 10 mA/g was used in 3rd, 10th, and 20th charge/discharge cycles, and a more rapid cycling current of 45 mA/g, to determine cycle life, was used for cycles 4–9 and 11–19.

Results and Discussion

Structure analysis of ballmilled $C_{1-x}Si_x$ powder.—Figure 1 shows XRD patterns of ballmilled $C_{1-x}Si_x$ (x = 0–0.25) and unmilled $C_{0.6}Si_{0.4}$ powder. From Fig. 1 we see that the graphite and silicon in unmilled $C_{0.6}Si_{0.4}$ are very graphitized 2H graphite and well-crystallized silicon, respectively (see Fig. 1e). After 150 h of ballmilling, we observed a decrease in intensity as well as a broadening of the [002] carbon Bragg peak. The width of the [002] Bragg peak of carbon decreased with increasing content of silicon. The *Lc* of carbon increased from about 1.3 to 10 nm when the silicon content increased from 0 to 20 atom %, which indicated that the relatively hard and brittle silicon inhibits crumbling of the graphite crystallite regions. The interlayer distances (d_{002}) of carbon were 3.55, 3.46, 3.41, and 3.38 Å for ballmilled graphite, $C_{0.9}Si_{0.1}$, $C_{0.8}Si_{0.2}$, and $C_{0.75}Si_{0.25}$, respectively. All the values of d_{002} in ballmilled powder mixtures are larger than that of unmilled graphite (3.35 Å). The increase of d_{002} in ballmilled powder mixtures are larger than that of unmilled graphite (3.35 Å). The increase of d_{002} may be attributed to the interstitial carbon atoms being introduced into initially pristine graphite,[12] the interstitial carbon atoms lying between the aromatic planes of carbon atoms.[13] Aladekomo and Brag found that the interlayer spacing of ballmilled graphite increases in step with mechanical milling time,[12] and they attributed the increase in d_{002} to forming a carbon interstial phase. During mechanical ballmilling the graphite initially formed a solid solution with single carbon atoms and then transformed into metastable carbon interstitial phases characterized by spacing of 3.375, 3.4, 3.44, and 3.55 Å, which is similar to the behavior of a graphite intercalation compound (GIC).[12] The steps in the interlayer spacing are also observed in annealing of artificial carbon,[14] which demonstrated the existence of interstitial carbon atoms between the aromatic planes of carbon atoms in those materials.[14] Therefore, we believe that after 150 h of mechanical milling, the graphite

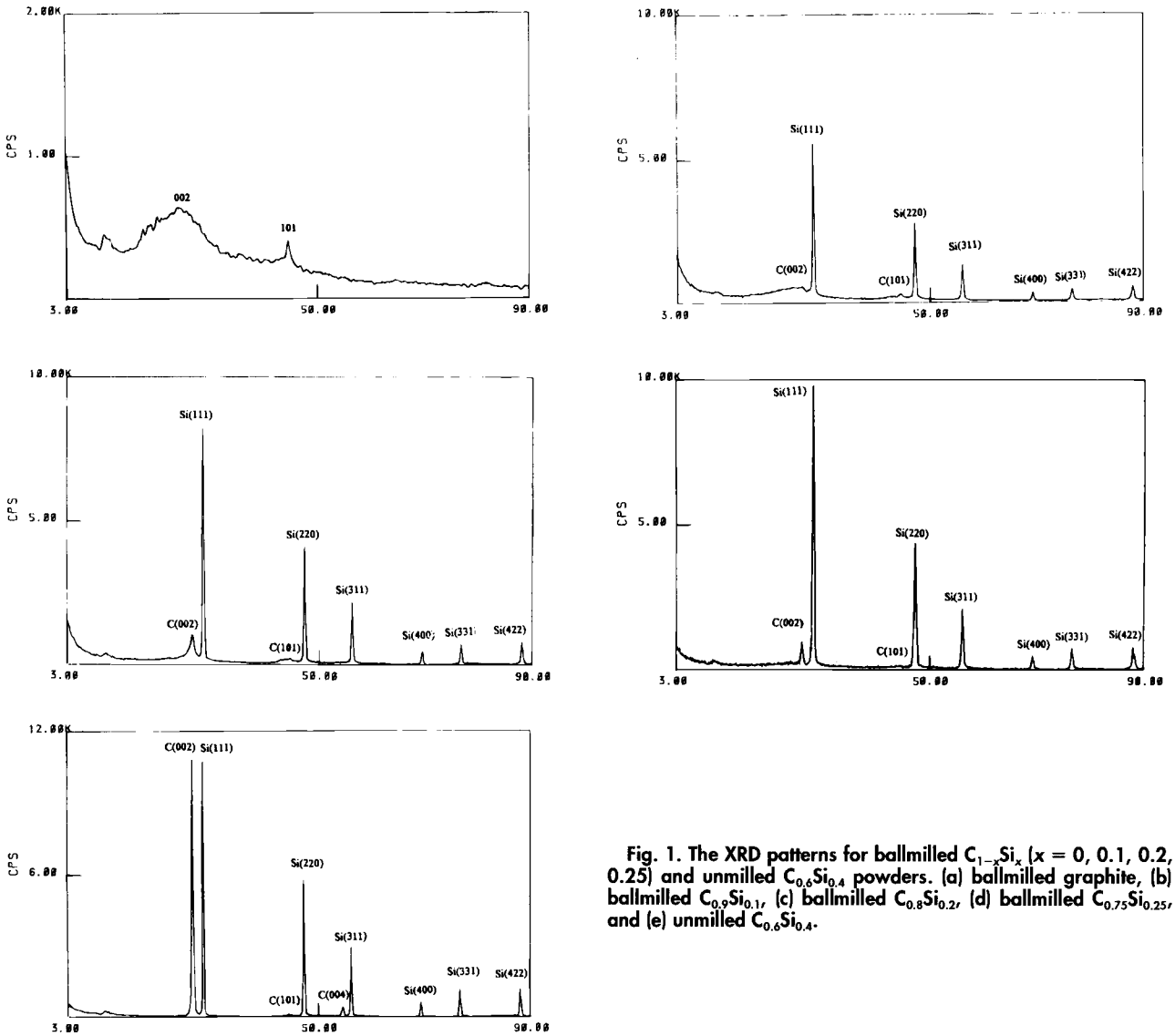

Fig. 1. The XRD patterns for ballmilled $C_{1-x}Si_x$ (x = 0, 0.1, 0.2, 0.25) and unmilled $C_{0.6}Si_{0.4}$ powders. (a) ballmilled graphite, (b) ballmilled $C_{0.9}Si_{0.1}$, (c) ballmilled $C_{0.8}Si_{0.2}$, (d) ballmilled $C_{0.75}Si_{0.25}$, and (e) unmilled $C_{0.6}Si_{0.4}$.

in $C_{1-x}Si_x$ powders was transformed into a metastable carbon interstitial phase and its structure is identical with those of carbonaceous materials obtained in pyrolyzing hydrocarbons.[14] Also, the decrease in d_{002} values with increasing content of silicon indicates that the silicon could inhibit the insertion of interstitial carbon atoms into the initial pristine graphite structure during ballmilling. It is noted that the values of Lc and d_{002} for ballmilled graphite are consistent with those reported by Aladekomo and Bragg,[12] but the present d_{002} is smaller than the result (d_{002} = 3.68) of Shen et al.[5] and larger than the result (d_{002} = 3.37 A) of Disma et al.[10] The possible interpretation for this is that the milling rate may vary considerably according to the nature of the ballmill process, the speed, and the charge, etc.[9] The milling rate may increase in order as follows: (*i*) 8:1 ball-to-powder ratio and 65 h of milling time (in Ref. 10); (*ii*) 12:1 ball-to-powder ratio, 270 rpm and 150 h of milling time (in the present paper); and (*iii*) 40:1 ball-to-powder ratio, 720 rpm and 40 h of milling time (in Ref. 5). Therefore it is reasonable to believe that a high milling rate would result in a large d_{002} value.

From Fig. 1 we can also see that the decrease in intensity of the [002] Bragg peak of graphite is greater than that of the [111] Bragg peak of silicon. A possible interpretation for this has been suggested to be due to the facile pulverization of graphite and its low mass-absorption coefficients for X-ray radiation.[15] After 150 h of ballmilling, a slight broadening of the [111] silicon Bragg peak shows that the size of the silicon crystallites also decreases during the ballmilling process. Another point worth mentioning is that no crystalline SiC phase peak was found under the present milling conditions. Yang and Shaw[9] believed that the collision energy and the method of milling significantly affect the product structures, and that there is a threshold collision energy. If the collision energy is either too low or too high, no crystalline SiC is produced.[9]

Laser Raman spectroscopy gives information about the vibration of atoms in crystals and molecules and can be used as a complementary tool to XRD. Figure 2 shows the Raman spectra of ballmilled $C_{1-x}Si_x$ (x = 0–0.25) powders. Two peaks are observed at about 1580 and 1360 cm^{-1} for each spectrum. The 1580 cm^{-1} band was assigned to the Raman-active E_{2g2} mode of graphite lattice vibration.[16] The 1360 cm^{-1} band is generally considered to originate from the disorganized region near crystal edges and lattice defects.[16] As is obvious from Fig. 2, the E_{2g2} band intensity increases with decreasing silicon content, and another Raman band at 1620 cm^{-1} appears to be present in the ballmilled graphite. We believe that the upward shift of the E_{2g2} band and the 1620 cm^{-1} bands arises from the vibration of carbon atoms near interstitial carbon atoms, because the interstitial carbon atom is bonded to one plane and atoms in the graphite plane are attracted to the interstitial area,[17] which may increase the force constant of carbon–carbon bonds in the plane at the interstitial region. If the force constant of carbon–carbon bonds becomes larger, the 1580 cm^{-1} of the graphite band would shift toward a higher frequency.[18] Therefore, the amount of interstitial carbon atoms may

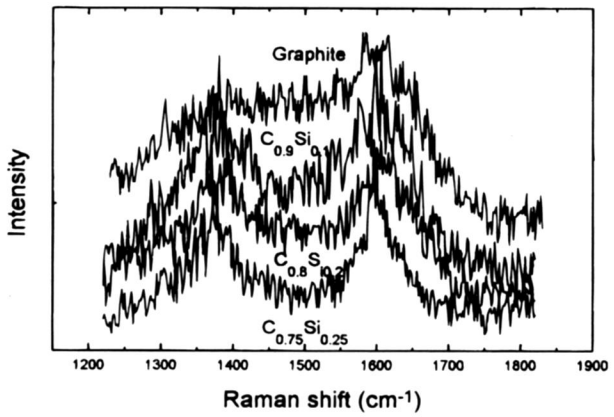

Fig. 2. Raman spectra of ballmilled $C_{1-x}Si_x$ (x = 0, 0.1, 0.2, 0.25) powders.

increase with decreasing silicon content due to the hard silicon inhibiting the pulverization of graphite. Also from Fig. 2 we can see that the bandwidths of both peaks broaden with decreasing silicon content, which indicates that the amount of imperfection and disorder in the carbon increases with decreasing silicon content. The information about ballmilled $C_{1-x}Si_x$ (x = 0–0.25) powders provided by Raman spectroscopy is in agreement with results obtained by XRD.

Microstructure observation of ballmilled $C_{1-x}Si_x$ powder.—Figure 3 shows bright-field HREM images of ballmilled $C_{1-x}Si_x$ (x = 0–0.20) powders. For pure graphite ballmilled for 150 h (Fig. 3a), the well-graphitized pristine graphite is pulverized into small particles in which there are numerous basic structural units (BSU) with a size about four unit cells thick and 1.4 nm lateral extent of graphite sheets (arrow a). In lattice images of [002] reflections of carbon, the layers are wrinkled, having irregular thickness and a distribution of interlayer spacings. The wrinkled layers could be attributed to the carbon interstitials, because the atoms in the graphite plane are attracted toward the interstitial region, but the nearest neighbors are forced in the opposite direction.[17] Dislocation loops are observed, thought to be regular "rafts" of interstitial atoms (arrow b), but may consist of loosely linked interstitial atoms each over or under rings in adjacent layers.[17] "Unorganized carbon" that may consist of bulk single layers or tetrahedrally bonded carbon[19] and microcavities could be formed among the edge of the BSUs. When 10 atom % silicon is mixed into the graphite, the BSUs are organized into distorted columns where they pile up much like bricks thrown into a heap (arrow c), that is, they tend to pile up approximately parallel but independently. The *Lc* of carbon increased to about

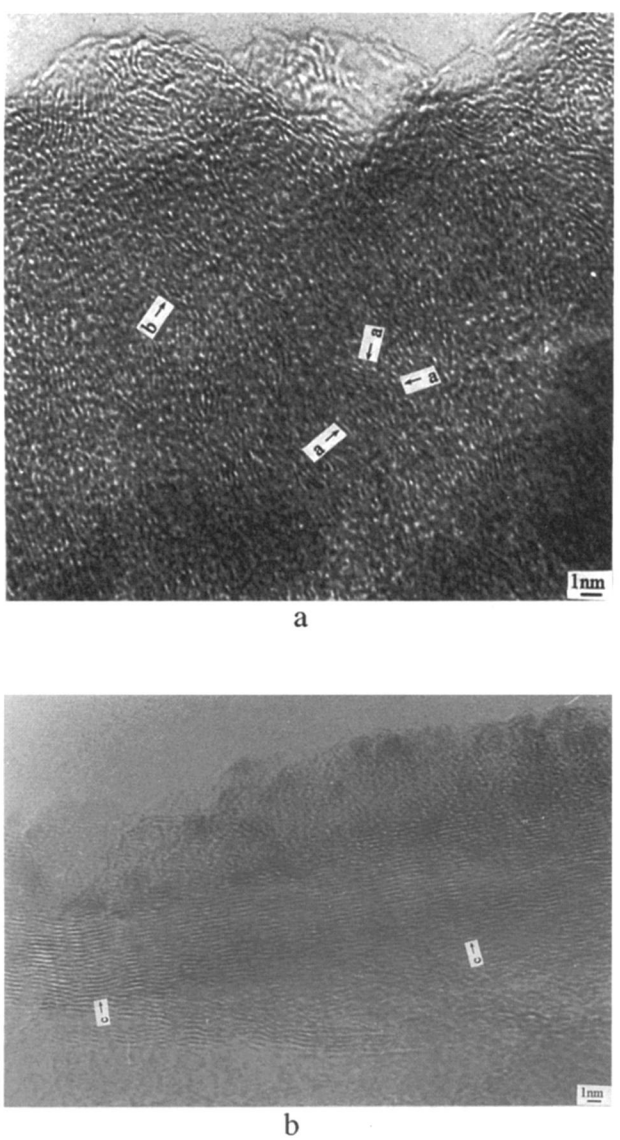

Fig. 3. HREM image for ballmilled $C_{1-x}Si_x$ (x = 0, 0.1, 0.2) powder: (a) ballmilled graphite, (b) and (c) ballmilled $C_{0.9}Si_{0.1}$, and (d) ballmilled $C_{0.8}Si_{0.2}$.

20 unit cells thick, and the lateral length of the graphite sheet, *La*, was about 1.5 nm in ballmilled $C_{0.9}Si_{0.1}$ powder (see Fig. 3b). The silicon also crumbled to about 40 nm, some amorphous silicon and dislocations were observed in the silicon of $C_{0.9}S_{0.1}$ powder, and the silicon is microencapsulated by thin amorphous carbon as shown in Fig. 3c.

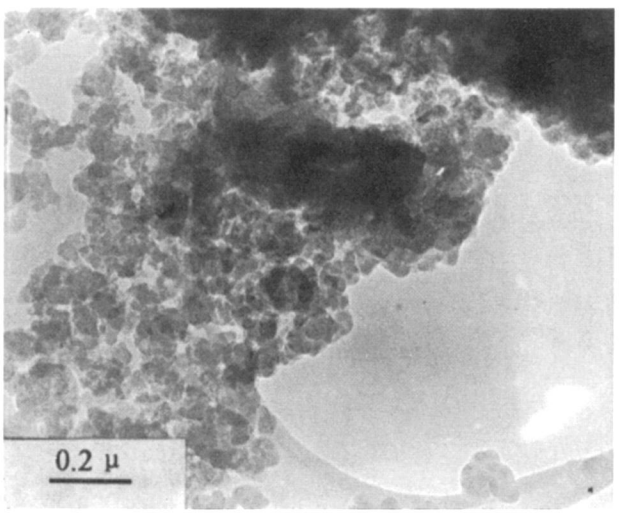

a

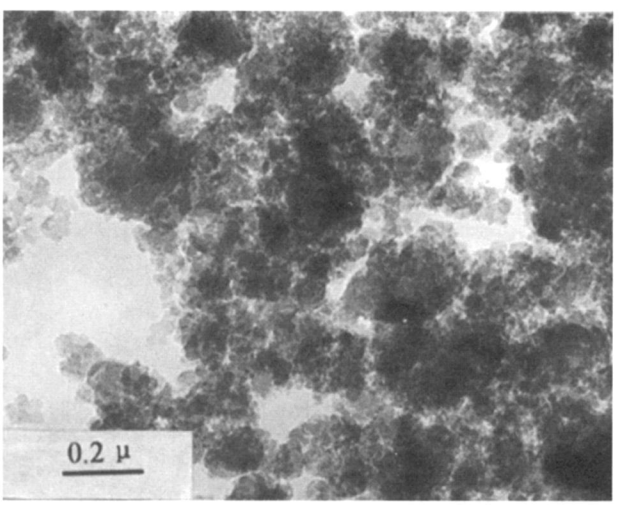

b

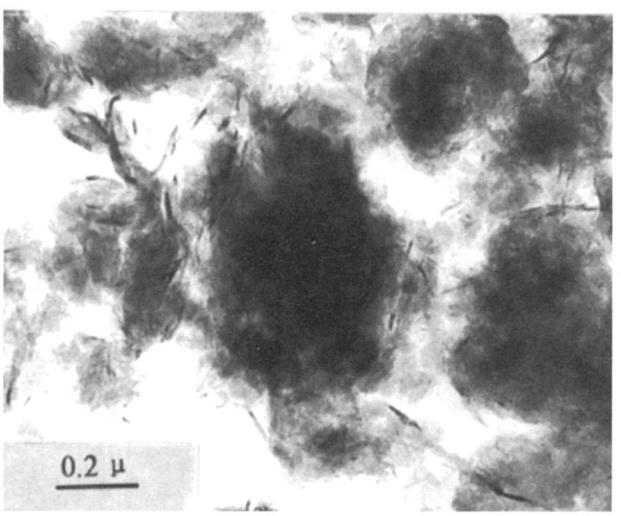

c

Fig. 4. TEM image of ballmilled $C_{1-x}Si_x$ (x = 0, 0.1, 0.2) powders: (a) ballmilled graphite, (b) ballmilled $C_{0.9}Si_{0.1}$, and (c) ballmilled $C_{0.8}Si_{0.2}$.

When the content of silicon was increased to 20 atom %, the crystal size of graphite La increased to about 10 nm, but the size of the silicon decreased to about 10 nm (see Fig. 3d). The possible interpretation for these observations is that when the content of graphite is high, the lubrication of graphite inhibits the crumbling of silicon, and when the content of silicon is high, the hard silicon slows the pulverization rate of graphite.

Morphology analysis of ballmilled $C_{1-x}Si_x$ powder.— TEM images of ballmilled $C_{1-x}Si_x$ powders are shown in Fig. 4. Note a change in powder morphology depending on the content of silicon. In ballmilled pure graphite, we observed the graphite being pulverized into small particles with an average mean diameter of 50 nm, and these particles agglomerate and result in lamella particles with an average mean diameter of about 1 μm and thickness about 0.6 μm. Voids are formed among the particles (see Fig. 4a). When 10 atom % silicon is added into graphite, the size of the agglomerated particles decreases to about 0.5 μm (see Fig. 4b). Upon increasing the content of silicon to 20 atom %, the agglomeration of particles is not clearly observed, but some larger graphite sheet are clearly seen (Fig. 4c), which confirms again that the hard silicon slows the pulverization rate of graphite.

Charge and discharge of ballmilled $C_{1-x}Si_x$ materials.— Figure 5 shows the first charge and subsequent charge/ discharges of unmilled graphite, $C_{0.6}Si_{0.4}$ powder, and ballmilled $C_{1-x}Si_x$ powder (x = 0, 0.1, 0.2, 0.25). In order to better reveal features of the potential plateaus, dQ/dV vs. V (differential capacity) plots for first charge/discharge for unmilled graphite and ballmilled $C_{1-x}Si_x$ (x = 0, 0.1, 0.2, 0.25) samples are shown in Fig. 6. For graphite it can be seen in Fig. 6 that the well-defined reduction/oxidation peaks observed in the dQ/dV plot reminiscent of a well-known staging phenomenon in unmilled graphite during lithium insertion/extraction disappears, but a potential hysteresis of about 1 V appears after 150 h of ballmilling. For $C_{1-x}Si_x$ (x = 0, 0.1, 0.2, 0.25) samples with increasing the silicon content the discharge peak near 1.15 V potential becomes weak and smooths out upon the silicon content increasing above 20 atom % (see Fig. 6b). However, the potential hysteresis of ballmilled $C_{1-x}Si_x$ (x = 0.1, 0.2, 0.25) were still larger than unmilled graphite but smaller than for ballmilled graphite (Fig. 5), and a new potential plateau at about 0.4 V appeared in the discharge curves (Fig. 6b). The bulk of the reversible capacity located near 0.4 V corresponds to Li extraction from the silicon.[4] The 1 V of potential hysteresis may be induced by interstitial carbon atoms between the aromatic planes of carbon atoms, because the interstitial carbon atoms bond to the carbon atoms in aromatic planes. When inserted Li diffuses to the interstitial

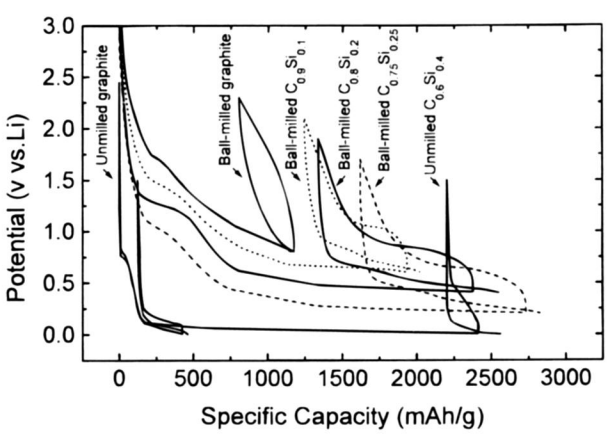

Fig. 5. The first charge and subsequent charge/discharges of unmilled graphite, $C_{0.6}Si_{0.4}$ mixed powder, and ballmilled $C_{1-x}Si_x$ powders (x = 0, 0.1, 0.2, 0.25). The data are offset sequentially for clarity. The shifts are 0.20, 0.40, 0.60, and 0.80 V for ballmilled $C_{0.75}Si_{0.25}$, $C_{0.8}Si_{0.2}$, $C_{0.9}Si_{0.1}$, and $C_1Si_{0.0}$, respectively.

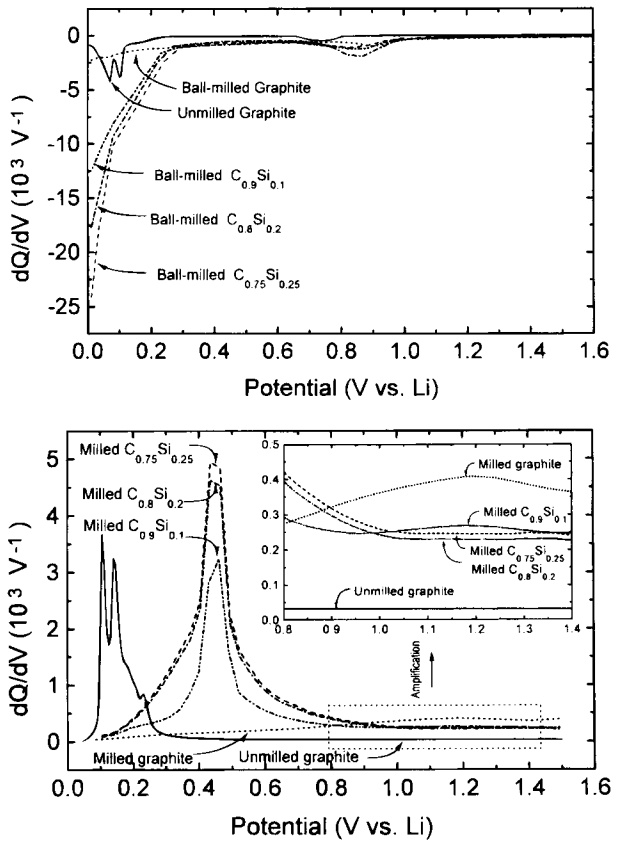

Fig. 6. Differential capacity of samples plotted vs. potential: (a) first Li insertion into samples and (b) first Li extraction from samples.

carbon atom, Li may transfer part of its 2s electron to a nearby interstitial carbon atom, resulting in a change of the bond between the interstitial carbon atoms and carbon atoms in aromatic planes. Li bonding to the interstitial carbon atom would cause a change in the relative atomic position of interstitial carbon. These bonding changes would be activated processes, which can lead to hysteresis.[20] Based on XRD, Raman, and HREM analyses and differential capacity curves for ballmilled $C_{1-x}Si_x$, we found that both the amount of interstitial carbon atoms and the peak intensity of differential capacity at 1.15 V decrease with increasing silicon content which indicates that the 1 V of potential hysteresis appears only when the amount of the interstitial carbon atoms exceeds a critical value. By careful examination of Disma and co-workers' results for Li insertion and extraction in ballmilled soft carbon,[10] we found that the 1 V of potential hysteresis appeared only after a certain ballmilling time. It is logical to believe that the amount of interstitial carbon atoms increases with increasing ballmilling time. Therefore, the results of Disma et al. corroborate our hypothesis. Also, for graphite both reversible and irreversible capacities rise after 150 h of ballmilling. The reversible and irreversible capacities are 300 mAh/g, 125 mAh/g for unmilled graphite, and 437 mAh/g, 739 mAh/g for ballmilled graphite (Fig. 7). The high reversible capacity for ballmilled graphite is probably due to Li insertion into vacancies, microcavities, and voids formed by ballmilling,[12] and the larger irreversible capacity is attributed to high surface areas of ballmilled graphite on which electrolyte decomposes, resulting in the formation of a passivating film or solid electrolyte interphase (SEI).[10] The irreversible capacities for milled and unmilled graphite are larger than those reported by Disma et al.[10] The higher irreversible capacities in the present study may be caused by the large amount of PTFE in our anodes, because PTFE as a binder would induce additional irreversibly capacity. As for ballmilled $C_{1-x}Si_x$ both reversible and irreversible

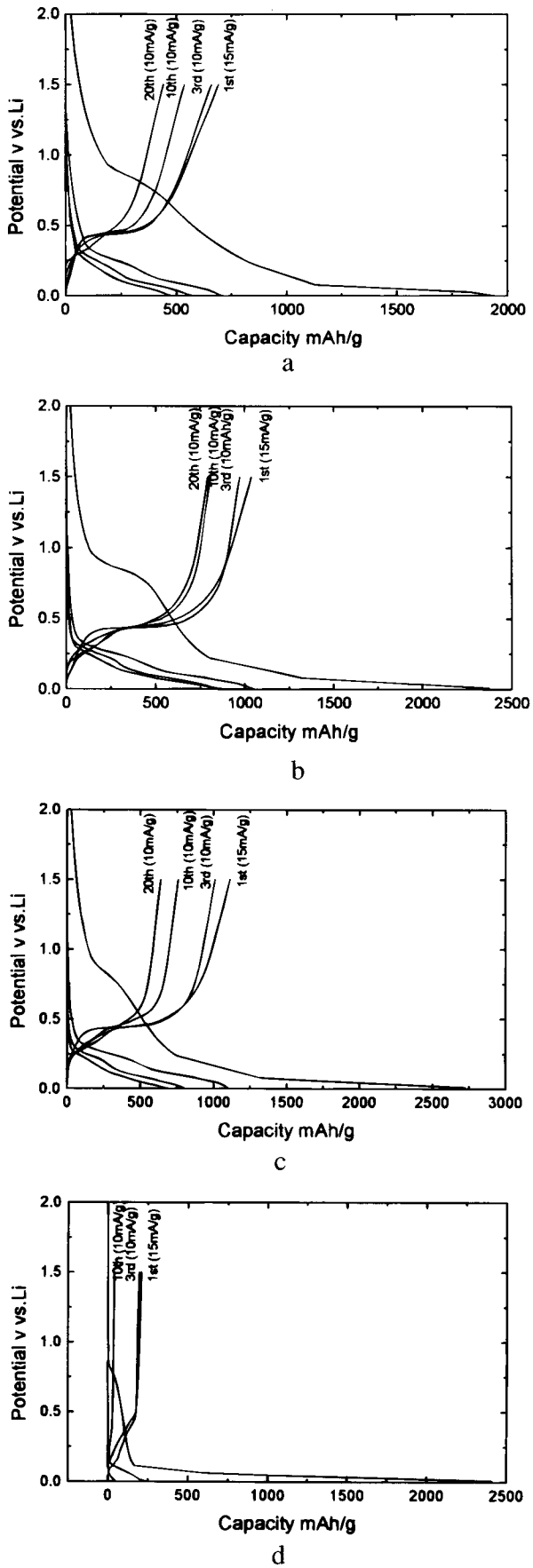

Fig. 7. Reversible and irreversible capacities of ballmilled $C_{1-x}Si_x$ powders as a function of the content of silicon. The reversible and irreversible capacities of unmilled graphite and $C_{0.6}Si_{0.4}$ powders are also shown for comparison. The solid line and dashed line are linear fits to the reversible and irreversible capacities of ballmilled $C_{1-x}Si_x$ powders, respectively.

capacities increase with increasing content of silicon, as can be observed in Fig. 7. But for ballmilled $C_{1-x}Si_x$ the reversible capacities are higher and irreversible capacities are lower than that for the unmilled $C_{0.6}S_{0.4}$ sample. The reason for this can be explained by the coexistance of nanosize silicon and very ductile graphite in ballmilled $C_{1-x}Si_x$ (x = 0.1, 0.2, 0.25) samples. It is well known that the Li insertion into silicon to form $SiLi_4$ can significantly increase volume by 323%,[21] which results in crumbing of Si–Li alloy. The cracks and powdering of silicon increase the contact impedance in the electrode and reduce the amount of lithium available for insertion and extraction in silicon during both storage and cycling. Therefore, the crumbing of silicon would decrease the reversible capacity but increase the irreversible capacity. However, when the silicon size is very small (nanosize) the crumbling rate may become very slow. Further, in ballmilled $C_{1-x}Si_x$ (x = 0.1, 0.2, 0.25) samples the nanosized silicon particles are separated and microencapsulated by soft and ductile carbon (Fig. 3c). At the start of lithium insertion, only silicon is expanded and becoming brittle, whereas the partly lithiated graphite still remains relatively soft and ductile, which decreases the crumbing rate of $C_{1-x}Si_x$ (x = 0.1, 0.2, 0.25) samples. The advantage of a very small particle-size multiphase Li-alloy anode (nanomaterials) for lithium insertion has been demonstrated recently also for tin-based metallic materials.[3] Furthermore, the irreversible capacities of ballmilled $C_{1-x}Si_x$ (x = 0.1, 0.2, 0.25) samples increase approximately in proportion to silicon content (dashed line in Fig. 7), and the irreversible capacities of ballmilled $C_{1-x}Si_x$ samples are also mainly due to Li irreversible insertion into silicon, because the irreversible capacities at about 0.6 V are more or less similar for all the ballmilled $C_{1-x}Si_x$ samples (Fig. 5 and 6a). In Fig. 7 the larger irreversible capacity than the value indicated by the dashed line may signal the higher crumbling rate of silicon during Li insertion/extraction. The slightly higher irreversible capacity of $C_{0.9}Si_{0.1}$ and $C_{0.75}Si_{0.25}$ than the value of the dashed line may be due to the larger size of silicon particles in $C_{0.9}Si_{0.1}$ and higher content of silicon in $C_{0.75}Si_{0.25}$ powder, because the irreversible capacity may increase with increasing content and size of silicon particles. For all samples the irreversible capacity due to the crumbing of silicon increases in the order of (see Fig. 7)

Ballmilled graphite < Ballmilled $C_{0.8}Si_{0.2}$
< Ballmilled $C_{0.75}Si_{0.25}$ < Ballmilled $C_{0.9}Si_{0.1}$
< Unmilled $C_{0.6}Si_{0.4}$

Also from Fig. 7 it can be seen that the reversible capacity of ballmilled $C_{1-x}Si_x$ powders increases from 437 mAh/g for ballmilled pure graphite to 1110 mAh/g for ballmilled

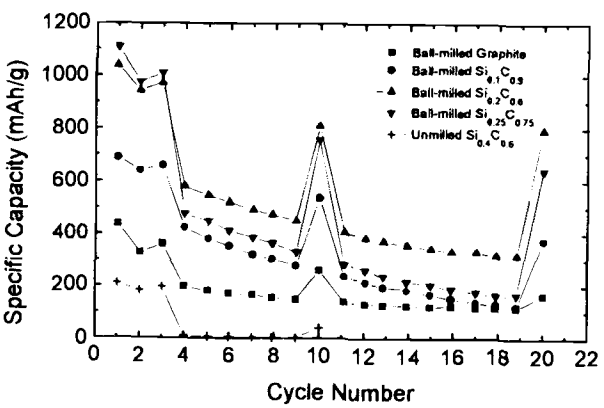

Fig. 8. Capacity vs. cycle number for ballmilled $C_{1-x}Si_x$ (x = 0, 0.1, 0.2, 0.25) and unmilled $C_{0.6}Si_{0.4}$ samples. For the first charge/discharge and second charge the electrode was cycled using a constant current of 15 mA/g. A lower cycling current of 10 mA/g was used in 3rd, 10th, and 20th charge/discharge cycles, and a more rapid cycling current of 45 mA/g to determine cycle life was used for cycles 4–9 and 11–19.

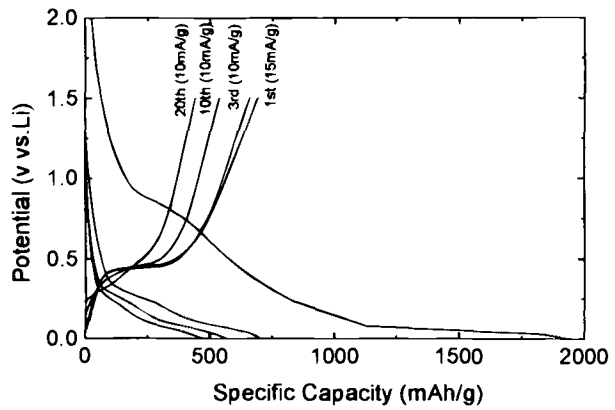

a

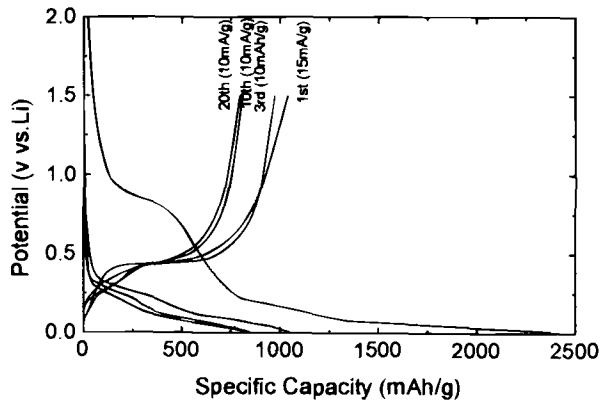

a

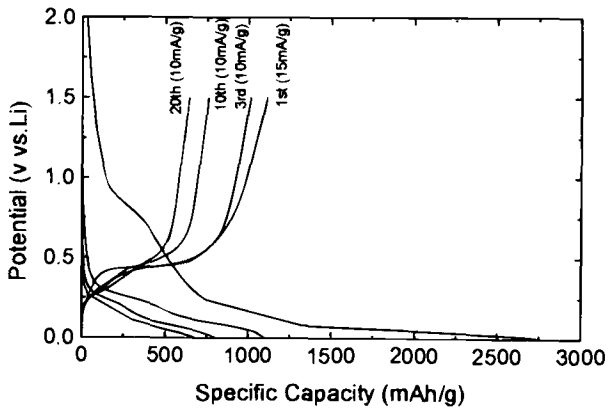

c

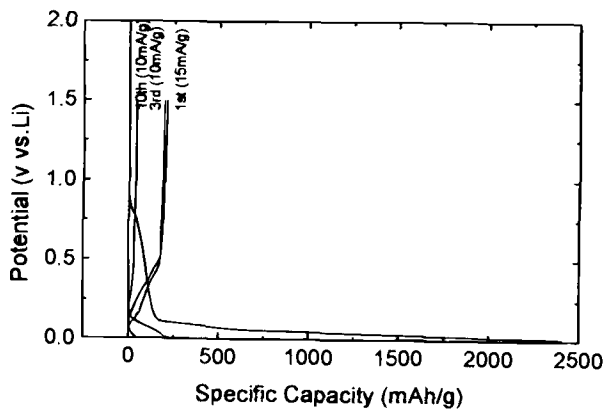

d

Fig. 9. The 1st, 3rd, 10th, and 20th charge/discharge curves of ballmilled $C_{1-x}Si_x$ and the 1st, 3rd, and 10th charge/discharge curve of unmilled $C_{0.6}Si_{0.4}$ samples: (a) milled $C_{0.9}Si_{0.1}$, (b) milled $C_{0.8}Si_{0.2}$, (c) milled $C_{0.75}Si_{0.25}$, and (d) unmilled $C_{0.6}Si_{0.4}$.

$C_{0.75}Si_{0.25}$ powders. The increase of reversible capacity with silicon content is approximately 30 mAh/g (atom % Si)$^{-1}$, which is in agreement with the results of carbons containing nanodispersed silicon prepared by CVD methods.[4] The observed slope in Fig. 7 suggests that each Si is alloying with ~1.5 Li atoms, which is lower than the maximum capacity of Li insertion into silicon ($SiLi_{4.4}$).[22] The reversible capacities of $C_{0.8}Si_{0.2}$ and $C_{0.75}Si_{0.25}$ electrodes are much larger than the capacity of carbons obtaining nanodispersed silicon (500 mAh/g) prepared by CVD[4] and polyvinyl chloride (PVC) (940 mAh/g) heated to 550°C.[23]

Cycle life of ballmilled $C_{1-x}Si_x$ powder.—The reversible capacities as a function of cycle number are compared in Fig. 8, and the 1st, 3rd, 10th, and 20th discharge curves of ballmilled $C_{1-x}Si_x$ and the unmilled $C_{0.6}Si_{0.4}$ electrode are shown in Fig. 9. In Fig. 8 we can seen that the cycle life decreases in order as follows

Ballmilled graphite > Ballmilled $C_{0.8}Si_{0.2}$

> Ballmilled $C_{0.75}Si_{0.25}$ > Ballmilled $C_{0.9}Si_{0.1}$

> Unmilled $C_{0.6}Si_{0.4}$

The cycle life is in reverse order of the irreversible capacity due to crumbling of silicon which indicates that the cycle life also depends on the crumbling of silicon. Further, for ballmilled $C_{1-x}Si_x$ electrodes the potential plateau at about 0.4 V gradually becomes more sloped and its width becomes shorter during charge/discharge cycling, (see Fig. 9), which indicates that some irreversible structural changes occur and the amount of Li extraction from silicon in the $C_{1-x}Si_x$ electrodes decreases. The limited cycling capacity is mainly related to the elimination of the capacity at 0.4 V, which reconfirmed that the cycle life is related to the crumbling of silicon. However, for the $C_{0.8}Si_{0.2}$ electrodes the decreases in reversible capacities become very slow after cycle 16 (Fig. 8), and the reversible capacity is still 794 mAh/g after 20 charge/discharge cycles, which suggests that this material is promising for anodes for Li-ion cells. In Fig. 8 one can also see that he rate capacities (i.e., high-rate dischargeability) of $C_{1-x}Si_x$ electrodes decreased with increasing silicon content, which may be due to a low diffusion coefficient of Li in silicon. In order to obtain the optimum content of silicon in $C_{1-x}Si_x$ electrode materials, a more detailed study of the relationship between the reversible capacity, rate capacity, the size, and content of silicon in $C_{1-x}Si_x$ electrode materials is needed. The study of effects of ballmilling conditions, including the mill design, milling speed, milling time, and ball-to-powder weight ratio on silicon size in $C_{1-x}Si_x$ and their electrochemical performance are in progress at our laboratory.

Conclusions

We prepared carbon containing nanosize silicon particles by ballmilling methods. The silicon and graphite were pulverized by ballmilling, and the silicon was microencapsulated by a thin layer of amorphous carbon. The nanosize silicon particles can reversibly insert lithium, which increases the capacity of the materials by taking advantage of the high lithium alloying capacity of silicon while retaining the high reversibility of carbon. $C_{0.8}Si_{0.2}$ ballmilled for 150 h had a reversible capacity of about 1039 mAh/g, which is three times the capacity of unmilled graphite. After 20 charge/discharge cycles the capacity remained at 794 mAh/g, which suggests that this material is a promising anode for Li-ion cells.

Acknowledgments

The authors acknowledge financial support from the National Nature Science Foundation of China (grant no. 59502005).

Manuscript submitted December 15, 1997; revised manuscript received May 1, 1998.

Zhejiang University assisted in meeting the publication costs of this article.

REFERENCES

1. I. A. Courtney and J. R. Dahn, *J. Electrochem. Soc.*, **144**, 2943 (1997).
2. J. O. Besenhard, P. Komenda, A. Paxinos, E. Wudy, and M. Josowicz, *Solid State Ionics*, **18, 19,** 823 (1986).
3. J. Yang, M. Winter, and J. O. Besenhard, *Solid State Ionics*, **90,** 281 (1996).
4. A. M. Wilson and J. R. Dahn, *J. Electrochem. Soc.*, **142,** 326 (1995).
5. T. D. Shen, W. Q. Ge, K. Y. Wang, M. X. Quan, J. T. Wang, W. D. Wei, and C. C. Koch, *Nanostruct. Mater.* **7,** 393 (1996).
6. M. Tidjani, J. Lachter, T. S. Kabre, and R. H. Bragg, *Carbon*, **24,** 447 (1986).
7. T. D. Shen, C. C. Koch, T. L. McCormick, R. J. Nemanich, J. Y. Huang, and J. G. Huang, *J. Mater. Res.*, **10,** 139 (1995).
8. B. B. Bokhonov, I. G. Kon Stancnuk, and V. V. Boldyrev, *J. Alloy Compd.*, **191,** 239 (1993).
9. Z. G. Yang and L. L. Shaw, *Nanostruct. Mater.*, **71,** 873 (1996).
10. F. Disma, L. Aymard, L. Dupont, and J.-M. Tarascon, *J. Electrochem. Soc.*, **143,** 3959 (1996).
11. J. Piscoe and B. E. Warren, *J. Appl. Phys.*, **13,** 364 (1942).
12. J. B. Aladekomo and R. H. Bragg, *Carbon*, **28,** 897 (1990).
13. M. Tidjani, J. Lachter, T. S. Kabre, and R. H. Bragg, *Carbon*, **24,** 447 (1986).
14. J. Lachter and R. H. Bragg, *Phys. Rev. B*, **33,** 8903 (1986).
15. L. L. Ye and M. X. Quan, *Nanostruct. Mater.*, **5,** 2 (1995).
16. F. Tuinstra and J. L. Koenig, *J. Chem. Phys.*, **53,** 1126 (1970).
17. J. Abrahamson and R. G. A. Maclagan, *Carbon*, **22,** 291 (1984).
18. M. Nakamizo, H. Honda, and M. Inagaki, *Carbon*, **16,** 281 (1978).
19. R. E. Franklin, *Proc. R. Soc. London, Ser. A*, **209,** 196 (1951).
20. J. R. Dahn, T. Zheng, Y. Liu, and J. S. Xue, *Science*, **270,** 590 (1995).
21. J. O. Besenhard, J. Gutler, and P. Komenda, in *Chemical Physics of Intercalation*, A. P. Legaud and S. Flandrois, Editors, NATOASI Series, Series B: Physics, Vol. 172, p. 469, Plenum Press, New York (1987).
22. A. Anani, S. Crouch-Baker, and R. A. Huggins, in *Lithium Batteries*, A. N. Dey, Editor, PV 87-1, p. 382, The Electrochemical Society Proceeding Series, Pennington, NJ (1986).
23. T. Zheng, Y. Liu, E. W. Fuller, S. Tseng, U. von Sacken, and J. R. Dahn, *J. Electrochem. Soc.*, **142,** 2581 (1995).